



Fargo: validation of space-relevant ferrofluid applications on the ISS

Saskia Sütterlin · Daniel Bölke · Manfred Ehresmann · Nicolas Heinz · Janoah Dietrich · Bahar Karahan, et al. [full author details at the end of the article]

Received: 3 March 2023 / Revised: 31 January 2024 / Accepted: 5 February 2024
© The Author(s) 2024

Abstract

The Ferrofluid Application Research Goes Orbital (FARGO) project desires to harness the potential of ferrofluids for advanced space system applications. Thereby, the student-led research project aims to develop, evaluate and subsequently validate three different ferrofluid-based applications on board the International Space Station (ISS): a novel attitude control system called FeroWheel as well as a Thermal and an Electrical Switch. The project is part of the Überflieger2 competition of the German Aerospace Center (DLR) in cooperation with the Luxembourg Space Agency (LSA). Central to this study is the role of ferrofluids in ensuring the functional principles to minimize the number of moving components ultimately. Therefore, the proposed systems have the potential to mitigate wear, reduce friction, and consequently improve the longevity and reliability of space systems. In the FeroWheel, a disc is supported on ferrofluid cushions instead of conventional ball-bearing-mounted rotors. This innovative approach, facilitated by the magnetic pressure positioning of the ferrofluid, eliminates the need for solid-to-solid contact. Circularly arranged coils function as the stator, propelling the disc with a 3-phase control, resulting in a spinning magnetic field. In addition to determining the generated torque, the objective is to validate experiments on system operations in which various acceleration and deceleration manoeuvres, as well as the stored angular momentum, are evaluated. The Electrical Switch leverages a self-manufactured magnetorheological fluid (MRF) developed by augmenting a liquid–metal base with iron powder. As a result, the fluid, akin to ferrofluid, has a magnetic field-responsive movement. Since a liquid metal is used as the base, the ferrofluid-like fluid acts as both the magnetically actuable and the current conducting fluid. To enable a current flow, the fluid is brought between the two electrical contacts utilizing electropermanent magnets (EPMs). These magnets combine the high magnetic field strengths of permanent magnets with the adaptive switching capability of electromagnets. Compared to all other demand-controlled magnetic field sources, this results in the great advantage that no energy is consumed as long as they are in one state. Only the switching process of the EPMS itself requires a high amount of energy, but only for a relatively short period. The switching behaviour under different loads will be investigated, evaluated, and compared to reference data recorded on Earth. The design of the Thermal Switch is characterized by the fact that it can be actively switched. Active thermal switching is still a relatively new field, so there is little comparative data from industrial solutions. Particularly for spacecraft, thermal design is crucial because the harsh environment of space must be taken into account. In addition to the challenge that heat can only be transferred to the environment via thermal radiation, severe conditions in space are characterized by extreme temperature differences. While extreme heat develops on the satellite surface on the side facing the sun, the opposite is valid on the shaded side. The resulting heat flow, which is irregular in time, location, and direction, leads to temperature peaks and gradients that can affect the system's performance, functionality, and reliability. Active switching provides selective control over heat transfer, allowing more flexible temperature regulation in critical areas and implementing a dynamic system response. Different design ideas are tested and evaluated for the applications in various experiments. The most suitable design is finally selected, further modified, and tailored for experimentation on the ISS and presented in this study. The most significant challenge is the time-critical factor of only a 1-year development phase. A total of 21 students from six different courses of study and two supervising PhD students from the Institute of Space Systems are involved in the FARGO project, all members of the small satellite student society at the University of Stuttgart, KSat e.V.

Keywords FARGO · Ferrofluid · ISS · Education · Microgravity research · Switch · ACS · Mechanic-free · FeroWheel

List of symbols

Br	Remanence	T
F_L	Load capacity	$\frac{N}{m^2}$
jH_c	Coercive field strength	A/m
I	Current	I
M_S	Magnetic saturation	T
t	Time	s
U	Voltage	V
λ	Thermal conductivity coefficient	W/mK
μ_0	Permeability of vacuum	$\frac{N}{A^2}$
η	Viscosity	mPa s

Abbreviations

ACS	Attitude control system
BDD	Behaviour driven development
BLDC	Brushless direct current
COTS	Commercial of the shelf
DLR	German Aerospace Center
DPG	German Physical Society
EPM	Electropermanent magnet
ESA	European Space Agency
ESC	Electronic speed controller
FARGO	Ferrofluid applications research goes orbital
FerrAC	Ferrofluid attitude control
GPIO	General purpose input/output
HCl	Hydrochloric acid
I2C	Inter integrated circuit
IRS	Institute of Space Systems at the University of Stuttgart
ISS	International Space Station
IR	Infra-red
LSA	Luxembourg Space Agency
KSat	Small Satellite Student Society at the University of Stuttgart
PAPELL	Pump application using pulsed electromagnets for liquid relocation
PCB	Printed circuit board
PCDU	Power control and distribution unit
PM	Permanent magnet
ppm	Parts per million
PTFE	Polytetrafluoroethylene
RPM	Revolutions per minute
RSEC	Reed–Solomon error correction
RTD	Resistance temperature detectors
SPI	Serial peripheral interface
STPA	System-theoretic process analysis
TRL	Technology readiness level
U	Unit

1 Introduction

Space is characterized by a harsh environment that presents myriad challenges. Extreme temperatures, radiation and micrometeoroids can challenge the reliability of space systems. Ensuring reliability in space missions is of paramount importance for several reasons. First, the significant investment in financial and human resources makes failures expensive and often politically sensitive. Second, reliability in human spaceflight is synonymous with crew safety. Finally, many space missions are once-in-a-lifetime opportunities—a failure could mean losing the opportunity to collect important data or explore a unique celestial body.

Mechanical moving components, in particular, are a critical source of failure due to their complex interactions and the space conditions mentioned above. In the past, the vulnerability of mechanical parts has been demonstrated in several space projects. For example, the Kepler space telescope and the FUSE, Dawn, and Hayabusa space missions all have one thing in common: the bearings of at least one of their reaction wheels failed on each of these spacecraft [1]. During the 1989 launch to explore Jupiter and its moons, the Galileo spacecraft's high-gain antenna failed to fully deploy, limiting the mission's data yield. The problem was attributed to the sticking of some antenna fins due to friction between their spacer pins and their sockets [2]. Such failures underscore the need to increase component longevity. As humanity's ambitions in space grow, so does the need to improve the reliability of the systems for space. This can also be seen in the effort that is being expended to estimate component reliability. For example, a list of data sources can be found in the Space Product Assurance prepared by the European Space Agency (ESA) [3, 4].

Consequently, developing systems with the lowest possible number of moving mechanical parts is a desirable goal. The possibility of reducing movable parts can be achieved by manipulating ferrofluid with magnetic fields. In this case, the particular functional principle of the component can be enabled by the use of ferrofluid. However, unlike their mechanical counterparts, which suffer from wear and tear due to constant physical contact, ferrofluid systems promise longer life with significantly less maintenance. Their ability to respond seamlessly to magnetic fields ensures not only precise control but also the potential for more compact and simpler design frames. As engineering challenges become increasingly complex, the comparative advantages of ferrofluid systems over conventional mechanical parts underscore their potential to revolutionize design methods for numerous applications.

In FARGO, an attitude control system called Ferrowheel, as well as a Thermal and Electrical Switch, are being



Fig. 1 Logo of the FARGO project

designed, developed and subsequently tested on the ISS. In Fig. 1, the logo of the project is shown.

1.1 Ferrofluid

In 1963, NASA aerospace engineer Stephen Papell conceptualized a fluid with distinct magnetic properties with the aim of designing a liquid rocket propellant that could be manipulated using external magnetic fields for efficient delivery to the combustion chamber [5]. Since then, ferrofluids have been continuously refined, leading to their incorporation into multifarious applications. Notably, these fluids have been employed as cooling mechanisms and to mitigate vibrations in audio loudspeaker systems, as well as in rotary shaft sealing [6].

Generally, ferrofluid consists of a carrier liquid, mostly a hydrocarbon-based oil, containing dispersed nanoparticles in the order of 10 nm. These nano-scale ferromagnetic particles are enveloped with surfactants to circumvent agglomeration. Owing to their nano-dimensional scale, they exhibit superparamagnetic characteristics. This entails that these particles encompass a singular magnetic domain, leading to a uniform magnetization [7]. Explicitly, in the absence of an external magnetic field, these nanoparticles remain demagnetized. Conversely, under the influence of a sufficiently strong external magnetic field, a magnetic response is elicited, characterized by the alignment of these nanoparticles and the magnetic manipulation of the fluid.

However, when exploring the potential of ferrofluids, the challenges posed by Rosensweig instability cannot be avoided. This phenomenon, which manifests itself as surface instability, occurs at the interface between two fluids, at least one of which is ferromagnetic. In this case, if an external magnetic field is applied perpendicular to the surface of the interface that exceeds a certain magnetic field strength, the

ferrofluid forms a structure of peaks and valleys, as clearly visible in Fig. 2. The peaks are usually arranged in a regular hexagonal pattern [8]. Overall, it arises from the interaction of several factors, like surface tension, magnetization, viscosity, and density interactions at the interface between the ferrofluid and the secondary fluid. Furthermore, an important aspect of the Rosensweig effect is its dependence on gravitational acceleration g . This dependence comes with a caveat: experiments conducted on Earth under the influence of gravity cannot be seamlessly transferred to microgravity or space. Moreover, since this instability is dependent on the particular secondary fluid, research into suitable secondary fluids was carried out, and is fully described in [9] and [10].

When selecting appropriate ferrofluids for the three distinct application experiments, it's crucial to evaluate each experiment individually due to their unique requirements:

- **Ferrowheel Experiment:** As detailed described in Sect. 2.1, the ferrowheel consists of a disk which rests on ferrofluid cushions. This disk has embedded permanent magnets to facilitate its structure. The ideal ferrofluid for this setup needs to possess the following:
 - **High colloid stability:** This ensures the ferrofluid's consistency when exposed to the magnetic flux density of the permanent magnets, which in turn ensures the ferrowheel's long-term reliability.
 - **Low viscosity:** A less viscous ferrofluid allows the disk to rotate more efficiently.
 - **A high magnetic saturation M_S** to increase the load capability of the ferrofluid bearing.

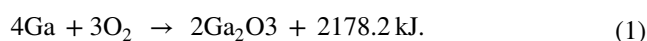
The ferrofluid EFH-1 from ferrotec is used in combination with distilled water, ethanol, and small amounts of sodium laureth sulfate [11], as preliminary tests demonstrated the best colloidal stability for this fluid combination.



Fig. 2 Pictures of the Rosensweig effect of ferrofluid, left with the ambient air as secondary fluid and in the right, with isopropanol. Underneath the petri dish left is a permanent magnet placed so that the magnetic field is perpendicular to the ferrofluid. The structure of peaks and valleys is visible

- **Electrical Switch:** This application demands at least two fluids.
 - **Conductive fluid:** When the switch is on, this fluid will facilitate the transport of electrical current.
 - **Insulating fluid:** This prevents current flow when the switch is turned off.
- **Thermal Switch:** Analogous to the Electrical Switch two fluids are required, but focused on heat conduction.
 - **Conductive Fluid:** Efficiently transfers heat when the switch is active.
 - **Insulating Fluid:** Halts heat transfer when the switch is off.

For both the Electrical and Thermal Switches, liquid metal has proven to be an effective choice as the conductive fluid in the “on” state. As documented in [12], among the various options tested, the combination of liquid metal, which can be magnetically actuated, emerged as the most efficient design for the switches. Depending on the specific requirements of each switch, an optimal insulating fluid can then be chosen. This innovative, self-manufactured fluid akin to ferrofluids has been deployed, as delineated in [13], with an amalgamation of 50 µm iron particles suspended in the liquid metal. However, due to the augmented particle size compared to standard ferrofluids, it is classified as a magnetorheological fluid (MRF). The aforementioned liquid metal, denoted as Galinstan, is a ternary alloy comprising gallium, indium, and tin. The fluid combines the metallic properties of Galinstan with the attribute of ferrofluid to react to magnetic fields. This allows the development of novel applications that require high and stable thermal and electrical conductivity, which is not present in general oil- or water-based ferrofluids. However, a critical aspect of using Galinstan is its sensitivity to oxidation. Oxygen in the environment, e.g. in the air, forms an oxidation layer. Due to the gallium content, the following reaction occurs [14]:



The thin Ga_2O_3 skin layer formed is characterized by pronounced viscoelastic properties, thus endowing the resulting material with rheological characteristics more akin to gels than conventional liquids [15]. The surface tension of Galinstan is relatively high, prompting it to minimize its surface area when undisturbed. As a result, a small amount of unoxidized Galinstan will form a sphere under the influence of gravity, as this shape is the most energetically favourable

state, enclosing the largest volume with the least surface area. However, when Galinstan oxidizes, it loses its ability to easily form this spherical shape due to its increased adhesion to surfaces. This oxidized layer makes it challenging to manipulate or actuate the liquid metal. Exposure to certain acids can reduce the oxidized layer, allowing the Galinstan to return to its spherical form, as seen in Fig. 3 on the right. In the Petri dish on the left, however, the oxidized skin layer is clearly visible.

Through various experiments with oxidized Galinstan and different concentrations of hydrochloric acid (HCl), it’s been determined that a 10% HCl solution effectively reduces the oxidized layer, allowing Galinstan to be stored for multiple weeks. However, due to their intrinsic conductive properties, acids are not recommended as insulating mediums for switches. To completely circumvent oxidation, the ambient atmosphere must contain less than one part per million (ppm) of oxygen [16]. Another critical aspect is that Galinstan forms an alloy with elemental aluminium. Tests with aluminium, which has its own oxide layer conventionally, show no alloying effects. Scratching the surface layer and exposing elemental aluminium below can be sufficient to start the process.

For the Electrical Switch, Galinstan-ferrofluid is used, combined with an insulating oil. In [17], different insulation fluids were tested in terms of their long-term stability, and the most suited was selected. For the Thermal Switch, on the other hand, it was not possible to develop a sufficiently closed enclosure to prevent the fluid from oxidation. Therefore, the same ferrofluid as in the FeroWheel is chosen with air as the insulation medium, knowing that there would be a high potential of improvement with a suitable housing. In the respective section of each experiment, in Sect. 2.1 for the ferrowheel, in Sect. 2.2 for the Electrical Switch and in Sect. 2.3 for the Thermal Switch, the selection criteria for the respective experiments are described in more detail.



Fig. 3 On the left is oxidized Galinstan, with a clearly visible skin layer appearing above one ppm oxygen content. On the right is a typical spherical liquid Galinstan droplet, hereafter reduction of the oxygen layer with hydrochloric acid

1.2 Magnetic field sources

In ferrofluids, despite the intrinsic ferromagnetic nature of the suspended iron nanoparticles, the fluid overall demonstrates paramagnetic behaviour, rendering it magnetically inert in external environments [9]. When subjected to an adequately intense magnetic field, these particles orient themselves along the field lines. Nevertheless, it must be ensured that the colloidal stability of the fluid is not affected, as this would lead to agglomeration of the particles and subsequent sedimentation. To initiate the motion of the ferrofluid, a dynamic magnetic field is required. This can be generated by coils or a mixture of electromagnets and permanent magnets.

In the case of the Ferrowheel, the motion of the ferrofluid is generated by an oscillating 3-phase current in the stator coils. The Switches, on the other hand, are utilizing customized electropermanent magnets (EPMs). In contrast to the electromagnets and permanent magnets used, these devices are not commercial of the shelf (COTS) components and are manufactured for FARGO itself. Therefore, they are further explained in the following.

1.2.1 Electropermanent magnet

An electropermanent magnet (EPM) is a specially designed combination of two cylindrical rods of permanent magnets (PM)—one fabricated from a soft magnet (SM) and the other from a hard magnet (HM). The soft magnetic alloy is composed of aluminium, nickel and cobalt (AlNiCo), while the hard magnet comprises an alloy of neodymium, iron, and boron (NdFeB). These PMs are aligned adjacently, with pole pieces constructed of the soft magnetic material Permenorm 5000 V5 from Vacuumschmelze affixed at both ends to guide the magnetic field [18]. Depending on the polarization of the soft magnet, the magnetic field’s trajectory alters, determining the EPM’s “on” or “off” state. When the polarities of both magnets are harmonious, the magnetic field courses through the pole pieces, activating the EPM. Conversely, with discordant polarities, the magnetic field is localized between the PMs via the pole pieces, deactivating the EPM [19].

Compared to all other demand-controlled magnetic field sources, the EPM has the great advantage that no power is consumed as long as it is in one state (“on” or “off”). Only the switching process of the EPM necessitates a transient yet high power surge—for FARGO’s EPMs, this equates to roughly 100 W in the low microsecond realm [12]. This characteristic of being an actively switchable permanent magnet is attributed to the nearly identical remanence B_r of the paired permanent magnets but with a marked disparity in their coercive field strength jH_c [19], listed in Table 1. This permits the SM to attain an inverse magnetization without perturbing the magnetic field of its HM counterpart.

In Fig. 4, the EPM’s polarity switching mechanism is elucidated. To modulate the SMs polarization, a coil encircles both magnets. Supplying a specific current facilitates magnetic saturation of an opposing polarity while preserving the remanence B_r of the soft magnet in its “on” state.

In the Electrical Switch, only a small drop of the Galinstan-ferrofluid is moved between the electrical contacts. Since there are no other requirements for the shape and size of the droplet, as long as it covers the two contacts sufficiently, an EPM of smaller dimensions can be built, referenced below as EPM4. In the Thermal Switch, on the other hand, heat flow can only occur efficiently if the area between the heat pipes is sufficiently filled with ferrofluid. For this reason, a larger EPM is used for this significantly larger droplet, referenced as EPM10. In Fig. 5 the two EPMs are shown in their basic geometries. Especially for the Electrical Switch the shape of the pole shoes is adapted to the design, explained in more detail in Sect. 2.2.

As the AlNiCo has to be magnetised in the opposite direction and not demagnetised, the current through the coil must be proportional to twice the coercivity jH_c listed in Table 1, which equals for both configurations approximately 5–6 A. The time required for a sufficient current pulse is dependent on the supplied voltage. For example, a voltage supply of 22 V requires a 15 μ s current pulse for the EPM4, whereas the EPM10 requires 228 μ s. This can be reduced to 7 μ s for the EPM4 and 84 μ s for the EPM10 by applying 34 V.

Table 1 Geometrical data and properties of the different PMs respective to the EPM configuration

Property	Unit	EPM4 _{SM}	EPM4 _{HM}	EPM10 _{SM}	EPM10 _{HM}
Diameter	mm	2 ± 0.1	2 ± 0.1	5 ± 0.2	5 ± 0.1
Length	mm	4 ± 0.1	4 ± 0.1	10 ± 0.1	10 ± 0.1
Manufacturing process	–	Cast	Sintered	Cast	Sintered
Coating	–	–	Ni–Cu–Ni	–	Ni–Cu–Ni
Curie-temperature	°C	860	310	860	310
Remanence B_r	T	1.26	1.32–1.37	1.24	1.32–1.37
Coercivity jH_c	$\frac{kA}{m}$	50.5	≥ 955	51.7	≥ 955

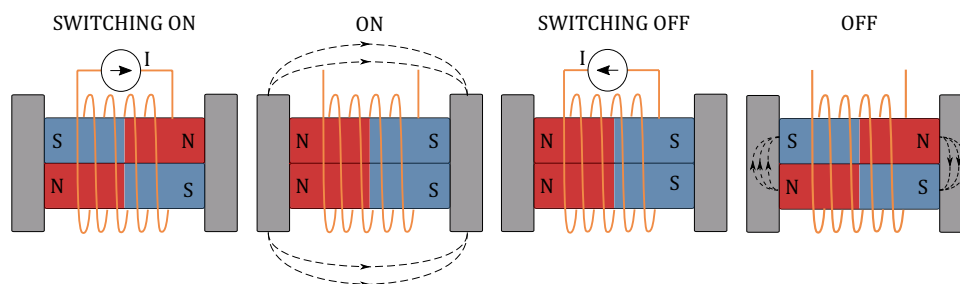
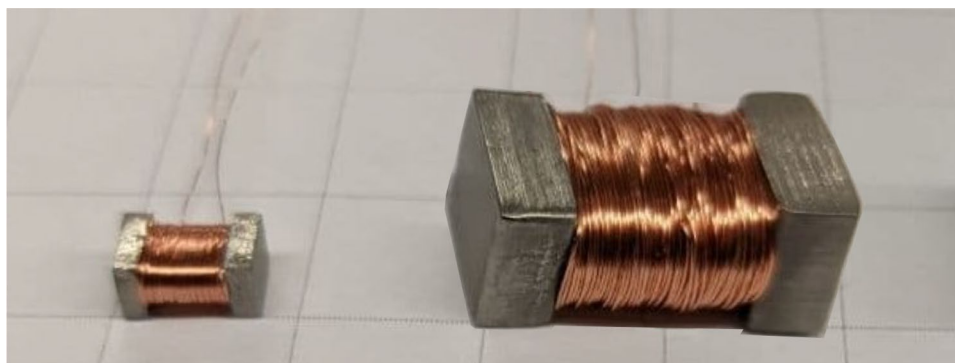


Fig. 4 Concept and switching process of an EPM. The magnetic field lines are represented by dotted black lines with arrows. In the top left picture, the EPM is switched *on*, whereby a directional magnetic field equivalent to the coercive field strength of the soft magnet is enabled via a defined current through the coil. In the *on* state, both PMs have

the same polarity therefore, the magnetic field lines are guided from each north to the south pole through the pole pieces attached at the ends. In the *off* state, however, the PMs are oppositely polarized, and the magnetic field lines are in a circle between the soft and hard magnet

Fig. 5 Picture of both EPM configurations: on the left, the EPM4 is shown, used for the Electrical Switch, whereas on the right, the EPM10 is shown. One grid equals 10 mm



1.3 Überflieger competition

Developing and testing the ferrofluid applications on the ISS is made possible by the Überflieger 2 competition organized by the German Aerospace Center (DLR) and the Luxembourg Space Agency (LSA). The prerequisite for the challenge was a successful participation in a two-stage application process. Besides FARGO, two more German [20, 21] and one Luxembourgian [22] teams were able to test their experiments on the ISS. The experiments are housed in a 2-unit CubeLab container of $20 \times 10 \times 10 \text{ cm}^3$ provided by Space Tango [23]. The mission time for testing the applications on the ISS is approximately 30 days. In addition, the experiments must be largely autonomous and not require any intervention by the astronauts. Fundamental research into the possibility of ferrofluid actuation in space was previously performed during the first Überflieger competition [24]. Since fundamental knowledge was gained in the development of ferrofluidic applications, the project PAPELL is presented in the following.

1.3.1 PAPELL

In the quest to extend the longevity of space applications, the manipulation and understanding of ferrofluids have become an important focus. A major effort in this area has been the project PAPELL (Pump Application using Pulsed Electromagnets for Liquid reLocation) from KSat, the small satellite student society at the University of Stuttgart. This technology demonstration, conducted in 2018 aboard the International Space Station (ISS), focused on understanding the behaviour and dynamics of ferrofluids under microgravity conditions. Over a period of 6 months with an operational period of more than 60 days, the team was successful in their endeavour [25]. The experiments examined the motions of ferrofluid in microgravity. This involved a range of manipulations, including droplet formation, motion, division, and merging, highlighting the essential features of fluid circulation in microgravity. Based on the promising results obtained at PAPELL, a working group on ferrofluid research was established at the Institute of Space Systems. In close cooperation with

KSat, several projects and final theses were carried out, which eventually led to Project FARGO [9, 12, 26–29].

2 Ferrofluid applications

In FARGO, three specific ferrofluid applications are tested, namely an attitude control system called Ferrowheel, a Thermal Switch and an Electrical Switch.

2.1 Ferrowheel

The Ferrowheel experiment delves into the mechanics of a brushless direct current (BLDC) motor, employing available COTS stators and an outrunner rotor. This stator, upon activation with alternating current (AC) supplied by an electronic speed controller (ESC), produces a three-phase magnetic field.

In the initial design phase, the experiment was purely fluidic, without any solid moving parts. This design involved the use of a ferrofluid droplet contained within a ring-shaped basin, accompanied by a suitable secondary liquid, as shown in Fig. 6. The changes in the stators' magnetic phases drive the acceleration of the ferrofluid droplet. However, the constraints imposed by the limited volume of the experimental cube did not seem to allow measurement of the achievable velocity, so the setup was not satisfactory for in-depth characterization. Complex measuring equipment is occasionally required to measure small torques.

The subsequent design iteration, also used as the flight experiment, introduced a rotor disc embedded with

permanent magnets (PM) that were saturated with ferrofluid. Here, the ferrofluid experiences a strong attraction towards the PMs, manifested as a magnetic pressure on the ferrofluid, which starts from zero at the fluid's surface and intensifies exponentially as it approaches the magnet's surface. Remarkably, the generated magnetic pressure allows the system to support a weight exceeding that of the magnet itself, with the load capacity of ferrofluid F_L with [30]:

$$F_L = \mu_0 M_S \int_S H dA, \tag{2}$$

with the vacuum permeability μ_0 , the magnetic saturation of the ferrofluid M_S and the magnetic field intensity H , integrated over the effective area of the pressure bearing pad S . As a result, a ferrofluid with a high magnetic saturation should be used. In the beginning, experiments were carried out with ferrofluids APG 313, APG CDF 2250 and EFH-1 from Ferrotec, among others. As can be seen in Table 2, the light hydrocarbon-based ferrofluid EFH-1 has twice the magnetic saturation of the other two ferrofluids APG 313 and APG CDF 2250.

The equilibrium established between this magnetic pressure and other prevailing forces paves the way for the creation of a passive, self-centering magnetohydrodynamic bearing.

All PM rings in the rotor are arranged in an alternating pattern to prevent residual dipole moments. For actuation, the permanent magnets are aligned in pairs, comparable to the magnetic configuration in a conventional motor rotor. In this pole pair arrangement, the magnetic field lines connect

Fig. 6 Picture of the first Ferrowheel concept that consists of no solid moveable components. A ferrofluid droplet, contained in a basin together with a suitable secondary liquid, is accelerated through a 3-phase AC of the stator



Table 2 Properties of different tested ferrofluids APG313, APG CDF 2250 and EFH-1 from ferrotec [31–34]

Property	Unit	APG313	APG CDF 2250	EFH-1
Carrier liquid	–	Synthetic hydrocarbon	Synthetic ester oil	Light hydrocarbon
Magnetic saturation M_S	mT	22	22	44
Viscosity	mPa s	152	500	6
Thermal conductivity	$\frac{mW}{mK}$	150	200	190

The properties viscosity and thermal conductivity are both at room temperature

and generate a strong local magnetic near field between the magnetic poles, while the magnetic far field is practically zero. The rotor will follow the alternating magnetic field produced by the stator. The rotor stores angular momentum, and thus, changes in the mean rotor velocity affect the angular momentum of structurally connected objects due to the overall conservation of angular momentum. The flight model of the Ferrowheel rotor is shown in Fig. 7. The stator is shown schematically centric of the Ferrowheel, and the 3-phase AC is indicated with the letters A, B and C in Fig. 7. On the right diagram, the curve of the three phases is shown.

The rotational speed, consequently, is measured via an encoder. As a result, the generated torque can be determined, which quantifies the currently achieved rotation rate of the system. From this, operational parameters are derived to

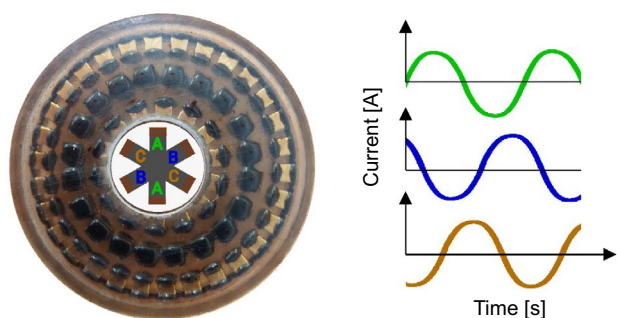
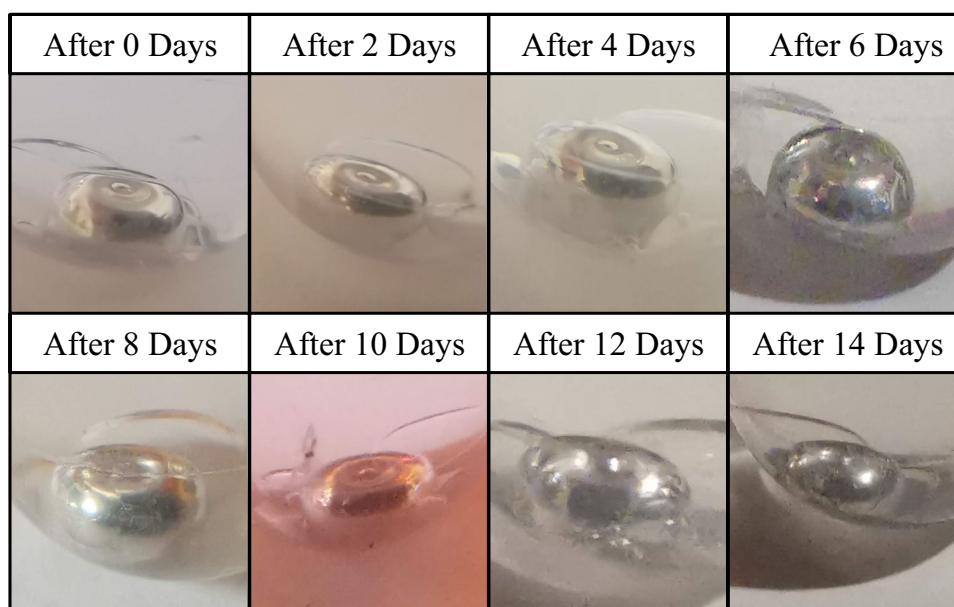


Fig. 7 Picture of the Ferrowheel concept with visible ferrofluid wetted permanent magnets and the concept of the three-phase stator in the middle. The stator is operated with three phases AC, indicated with A, B and C. The rotor is located around the stator with permanent magnets that have alternating north and south polarity, and are wetted with ferrofluid. In the right diagram, the curve of the three phases is shown

Fig. 8 Test of the fluid combination of transformer oil and Galinstan-ferrofluid to follow possible changes over time. No visible changes occur in the fluid combination



assess maximum storable angular momentum as well as operative torque able to be generated.

2.2 Electrical Switch

In the Electrical Switch, Galinstan-ferrofluid is used to close, or respectively open an electrical circuit. As already mentioned in Sect. 1.1, Galinstan has the challenge that it already starts to oxidize above 1 ppm oxygen concentration. For this reason, the insulation medium requires close attention to ensure that it has both a high breakdown voltage and a low oxygen concentration. Suitable mineral oils can have a significantly higher breakdown voltage compared to gases [35]. Furthermore, they facilitate handling compared to gases, as it protects the Galinstan-ferrofluid droplet from oxygen diffusion through the housing. Four different oils were tested for FARGO, including a silicone oil, a transformer oil, a kerosene oil and a Perfluoropolyether (PFPE) oil [17]. This involved storing a Galinstan-ferrofluid drop in sterile, vacuum-tight tubes in the oil and observing if any changes occurred. As observed in Fig. 8, no changes occurred in the tested transformation oil. In comparison, the changes in silicone oil can be clearly seen in Fig. 9.

Fluid combinations with silicone oil resulted in the most significant change in Galinstan-ferrofluid. Slight changes were seen in the PFPE oil. No changes were visible in the transformer oil or in the kerosene oil. For the Electrical Switch, the StaSo transformer oil from Starke Mineralölwerk has finally been selected as the most suitable insulating fluid, with a breakdown voltage of > 80 kV, determined according to IEC60156 [36].

Both fluids are contained within a specially designed Polytetrafluoroethylene (PTFE) tube, which also houses the

Fig. 9 Test of the fluid combination of silicone oil and Galinstan-ferrofluid to follow possible changes over time. As can be clearly seen, changes occur in the Galinstan-ferrofluid, making this combination unsuitable

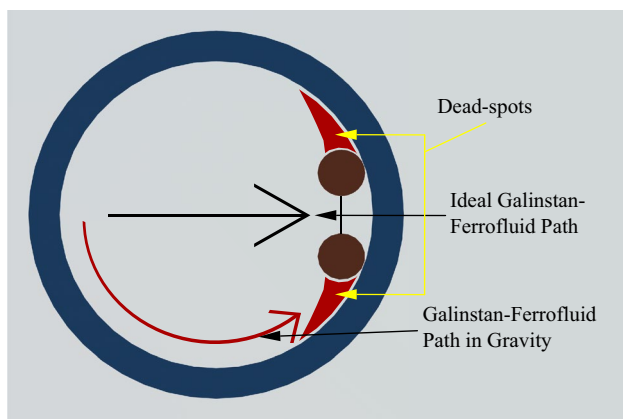
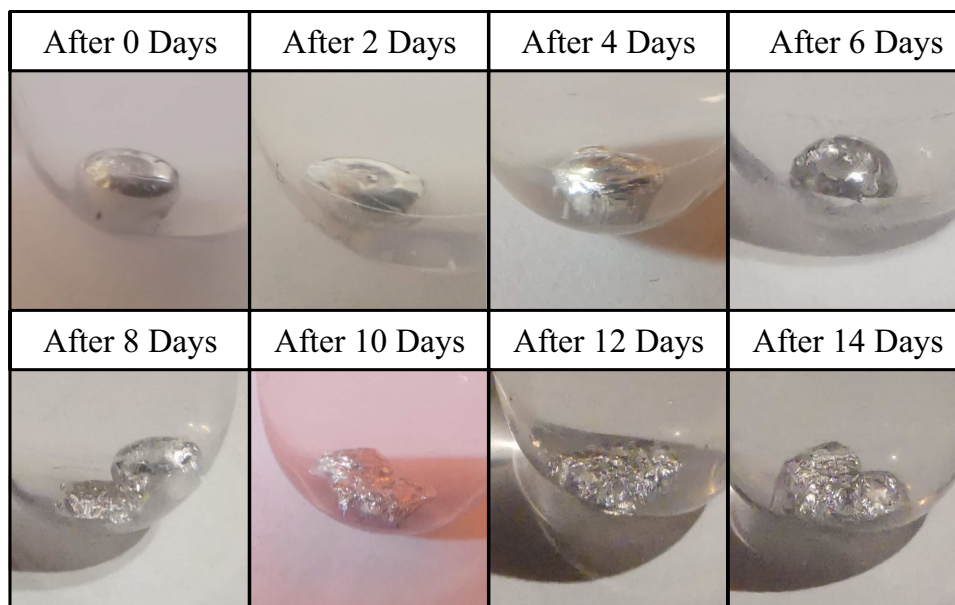


Fig. 10 This illustration provides the issues with a cylindrical tube’s cross-section. Red zones show possible areas where Galinstan-ferrofluid could get stuck. The black arrow points out the optimal course for the Galinstan-ferrofluid droplet, while a contrasting red arrow depicts its movement when affected by gravity

electrical contacts. Different tube shapes were explored to determine the best fit. In a cylindrical tube, the Galinstan-ferrofluid travels due to Earth’s gravity along a curved route at the tube’s rounded base, moving towards the contacts. This design allows the bottom contact to obstruct the Galinstan-ferrofluid from making contact with the upper electrical contact. Furthermore, the cylindrical design results in areas where the Galinstan-ferrofluid can get stuck and potentially remain indefinitely. The issues with the cylindrical tube are depicted in Fig. 10.

To circumvent the challenges with the cylindrical tube, a rectangular tube shape has been selected as the most promising shape.

To magnetically actuate the Galinstan-ferrofluid, two EPMs are mounted outside the rectangular tube. One EPM is placed beside the electrical contacts so that when this EPM is on, the droplet is attracted to the contacts. Both EPMs are cycled on and off so that the droplet moves to and surrounds the contacts, causing current to flow when the switch is on and moving away to insulate when the switch is off. For this purpose, the pole pieces of the EPMs were machined to effectively guide the magnetic field through the tube. In Fig. 11, the concept is shown in a cross-section view. The EPMs, marked with (1), are mounted on opposite sides of the switch. The Galinstan-ferrofluid droplet encased in the insulation fluid (2) can thus be pulled toward or away from the contacts (3). The green LED (4) on the right side can be used to visualize the current flow.

The switch is evaluated by monitoring the switching process of resistive, inductive, and capacitive loads with an oscilloscope. In addition, a camera is installed to detect the fluid movement.

Characterization tests were performed with an initial design of the Electrical Switch with a cylinder open at both ends. The tested values are listed in Table 3. For the electrical endurance test at nominal load, 2000 switching cycles were performed. In addition, the specifications of a normally closed (NC) reference reed relay JWD/JWS Series from Potter and Brumfield are listed for comparison [37].

By using EPMs, significant energy savings can be made compared to non-solid-state relays, as only the on-and-off switching process itself requires approximately 100 W for 30 μs. Compared to the reference relay, which consumes 10 W to maintain its on-state, the following obtains:

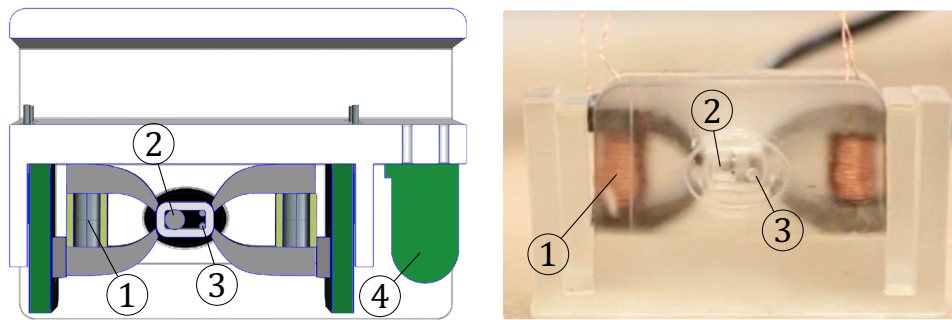


Fig. 11 Side view of the Electrical Switch concept. On the left, the schematic is shown, whereas on the right, a picture of the Electrical Switch can be seen. It is made up of two EPMs, marked with (1), a

droplet of Galinstan-ferrofluid as the conductive fluid contained in an insulating fluid (2), two electrical contacts (3), and a green LED to visualize the current flow (4)

Table 3 Electrical switch specifications of the developed switch as well as a reed relay as reference [37]

Property	Unit	Ferrofluid switch	Reed relay
Nominal voltage U_n	V	24	20
Nominal current I_n	mA	500	500
Maximum voltage U_{max}	V	100	100
Maximum current I_{inrush}	A	2	0.5
Electrical endurance at nominal load	Cycles	> 2000	$1 \cdot 10^6$
Switching power	W	Approx. 100	10
Minimum energisation duration	μ s	30 at 18 V	Continuous

$$100 \text{ W} \cdot 60 \mu\text{s} = 10 \text{ W} \cdot t_E \quad (3)$$

As a result, the developed Electrical Switch has an energy advantage over the reed relay when the state is held longer than $t_E = 0.6$ ms. On the other hand, test results show that the switch is not as sensitive to overload as solid-state relays (SSRs).

In addition, another long-time test of 2000 switching cycles was carried out with the final design. On average, a switch-on time of 12.45 ms and a switch-off time of 14.09 ms were achieved.

2.3 Thermal switch

The Thermal Switch is characterized by its ability to allow or prevent a heat flow in a controlled manner via heat conduction paths. For this purpose, as in the Electrical Switch, a combination of two fluids is used. A fluid with a high thermal conductivity λ should ensure that the heat flow across the fluid is enabled in the on-state of the Thermal Switch. In the off-state of the switch, on the other hand, an insulating fluid should prevent heat flow as best as possible. The operating principle is shown in simplified form in Fig. 12.

The Thermal Switch can be characterized by the proportionality between the heat flow \dot{Q} and the applied temperature difference ΔT . The respective heat flow of both states \dot{Q}_{ON} and \dot{Q}_{OFF} can then be determined to:

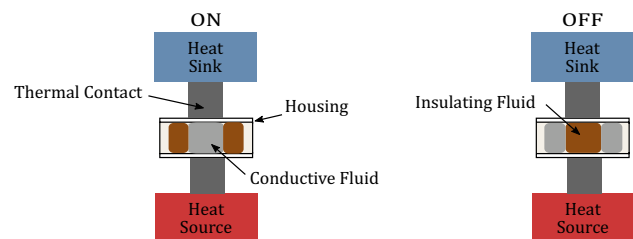


Fig. 12 Schematic operating principle of the Thermal Switch. In the left on-state of the switch, the thermally conductive fluid is used to allow heat flow, while in the right off-state, an insulating fluid is used to prevent heat flow

$$\dot{Q}_{ON} = A \cdot \lambda_{ON} \cdot \frac{1}{l} \cdot \Delta T_{ON}, \quad (4)$$

$$\dot{Q}_{OFF} = A \cdot \lambda_{OFF} \cdot \frac{1}{l} \cdot \Delta T_{OFF}. \quad (5)$$

The first design iterations with the Thermal Switch also envisaged the use of Galinstan-ferrofluid with nitrogen as the insulating medium. Due to the larger area that must be covered in the on-state, a more complex design is necessary. Therefore, the larger EPM 10 configuration is used, attached to both sides of the housing, and an additional coil is wound around the housing. First tests with copper

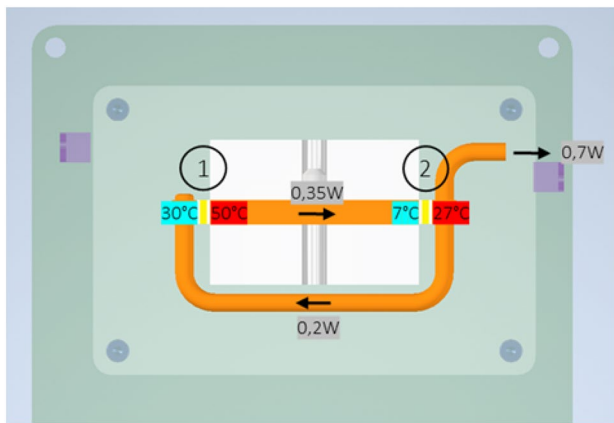


Fig. 13 Thermal simulation in the sectional view of the thermal switch experiments. The heat source is located at (1), while the heat sink is located at (2). To dissipate the heat, the rear of the Peltier elements is connected to a heat pipe. The calculations are based on the data sheet of the Peltier element and a circulating heat flow of 0.2 W. This results in a potential heat flow of 0.35 W via the switch in the on state

as heat conduction paths showed that the Galinstan adhered to the copper rods. As a result, silver rods were taken for the final design, with a half-spherical profile on each of the housing. One heat source and one heat sink are attached to each end, for which the thermoelectric coolers (TECs) NL1020T-01AC are used [38]. As shown in the thermal concept in Fig. 13, the TECs are set up in a heat transfer loop where the hot side of one is linked to the cold side of the other.

Additional power that needs to be dissipated from the switch to run the TECs is achieved via a thermal connection to the Tango Cube.

With the assumption of a constant heat flow applied by the TECs $\dot{Q}_{ON} = \dot{Q}_{OFF}$, the following applies for the switching ratio:

$$\eta = \frac{\Delta T_{OFF}}{\Delta T_{ON}} = \frac{\lambda_{ON}}{\lambda_{OFF}}. \tag{6}$$

Ultimately, it was not possible to efficiently actuate the Galinstan-ferrofluid droplet within the housing during the project design timeframe of approximately one year. Therefore, the hydrocarbon-based ferrowheel ferrofluid EFH-1 with a thermal conductivity listed in Table 1 as $190 \text{ mW}/(\text{mK})^{-1}$ as conductive fluid and air as insulation fluid were chosen. The final concept is shown in Fig. 14.

Tests on the ground with the final setup, plotted in Fig. 15, give a switching ratio of: $\eta > 1.04$. To process the obtained data of the Thermal Switch, a Savitzky–Golay filter using a window of 75 data points and a 5th-degree polynomial is applied [39].

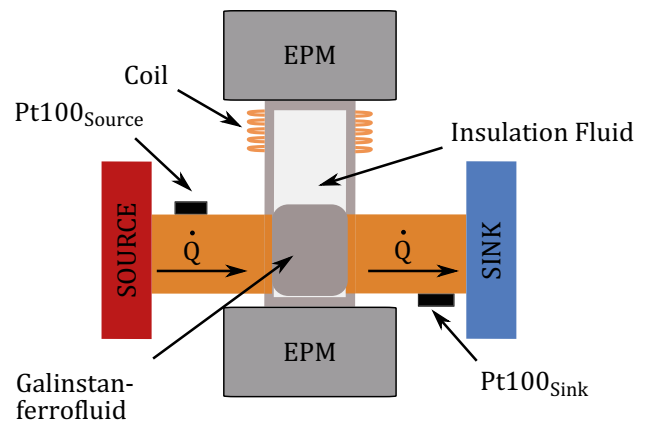


Fig. 14 Schematic drawing of the final Thermal Switch design. Electropermanent magnets (top and bottom grey box) are able to control the grey Galinstan-ferrofluid position. In the down position, a heat flow is enabled. In the up position, the switch acts thermally insulating

3 Experiment setup

The experiment setup is determined by the constraints and requirements of Space Tango’s CubeLab container. The implementation is carried out in the subsystems of mechanics, electronics and software.

3.1 Mechanics

The mechanical structure of the FARGO experiment is centred around easy integration, serviceability and the minimization of production costs. The structure of FARGO, housed in the CubeLab container is comprised of laser-cut aluminium panels fixed onto threaded rods that are rooted in the Space Tango Panel at the bottom of the Space Tango Module. The panels are tensioned via nuts and SLS 3D-printed steel frames provided by the Fraunhofer IPT. Each of the panels constitutes the mounting point for one of the experiments. The panel fixed directly above the Tango sled at the bottom carries the electronics, cabling and support infrastructure. The first layer of panels houses the Electrical Switch and the lower half of the Ferrowheel experiment, and the second layer is the base of the Thermal Switch experiment and the upper half of the Ferrowheel experiment.

The flight model can be seen in Fig. 16.

The materials used throughout the design were chosen for various criteria, mainly their weight and their workability in the available student workshops. Simple support parts and brackets are FDM 3D printed in PETG, and the containments are polyjet-printed. Structural parts are either steel or aluminium. As already mentioned, Galinstan forms an alloy

Fig. 15 Temperature difference ΔT plotted over time for a switching time of 45 s from previous measurements on Earth. On the right, the applied Savitzky–Golay filter is shown

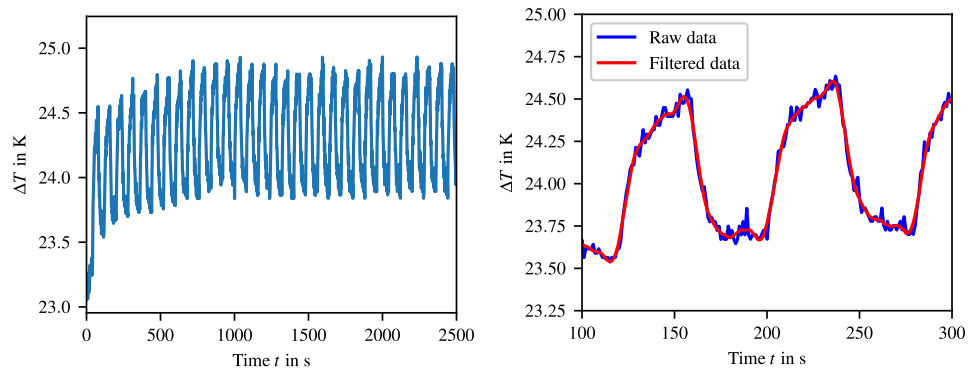
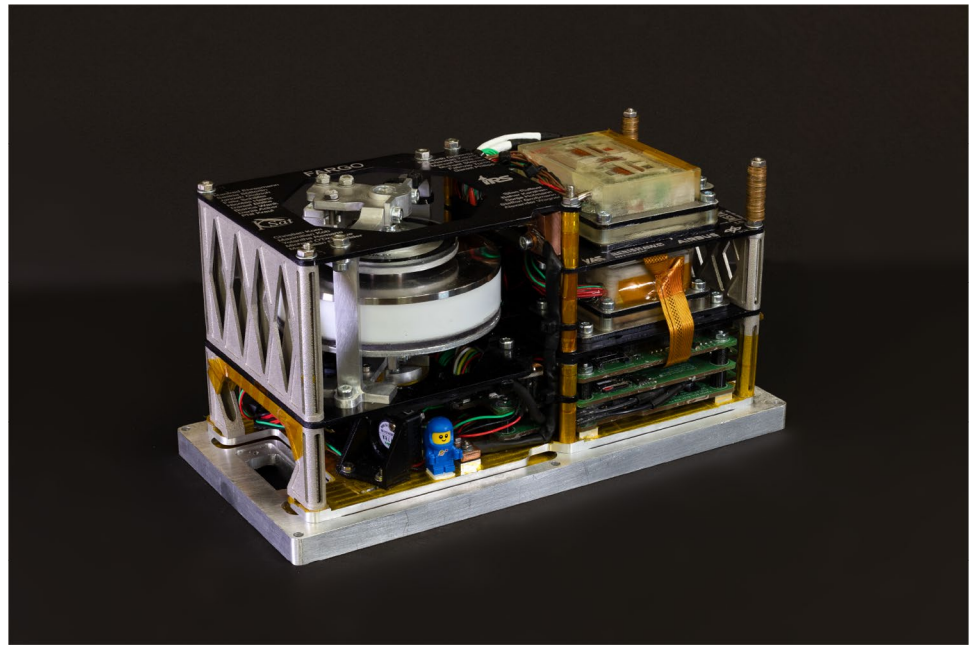


Fig. 16 The flight model of FARGO, the Ferrowheel experiment on the left, Thermal and Electrical Switch on the right



with aluminium and, in this way, poses a danger to both the structure as well as the Space Tango container. To alleviate this the aluminium panels were anodized and all structurally relevant parts were coated in Kapton.

To ensure the structural integrity of the complete structure and the experiments throughout the mission, a FEM analysis of the overall structure was performed. Furthermore, a vibration test of several critical parts, as shown in Fig. 17, was conducted at Airbus Defence and Space in Friedrichshafen using a representative launch profile.

3.1.1 ACS-experiment

The Ferrowheel is the most complex of the three experiments, its mechanical structure is briefly described from the inside out. An angled view of the CAD is shown in Fig. 18.

In the center of the experiment, the commercial stator is fixed to a steel shaft for thermal control. This shaft interfaces with a steel axle via a form-fitting. The stator

is housed in a milled PTFE housing that also contains the runner, which consists of a laser-cut steel panel that is equipped with permanent neodymium magnets for both the interface with the stator and the ferrofluid bearings. This runner is suspended in a secondary fluid. To contain the runner and the secondary fluid, the PTFE containment is closed with an acrylic cover that is supported by an aluminium frame. The acrylic cover allows for video monitoring of the runner, while the aluminium frame supports the cover during phases of high mechanical stress. Throughputs in the acrylic cover feed the cables from the stator into the hollow axle, through the ball bearing and then to a slip-ring. Two ball bearings secure the axis in place; they are secured with bearing retainers into a CNC-milled precision frame so that the fully assembled shaft with an integrated experiment module can be installed from the side to ease the integration process and the precision. The precision frame serves as a mounting point for the whole experiment, as well as the encoder and the slip-ring.

Fig. 17 The shaker test assembly at Airbus Defence and Space in Friedrichshafen. The test modules were fixed to a plate, which in turn was fixed to the vibration plate. In addition, various ferrofluid samples were tested for their vibration resistance.

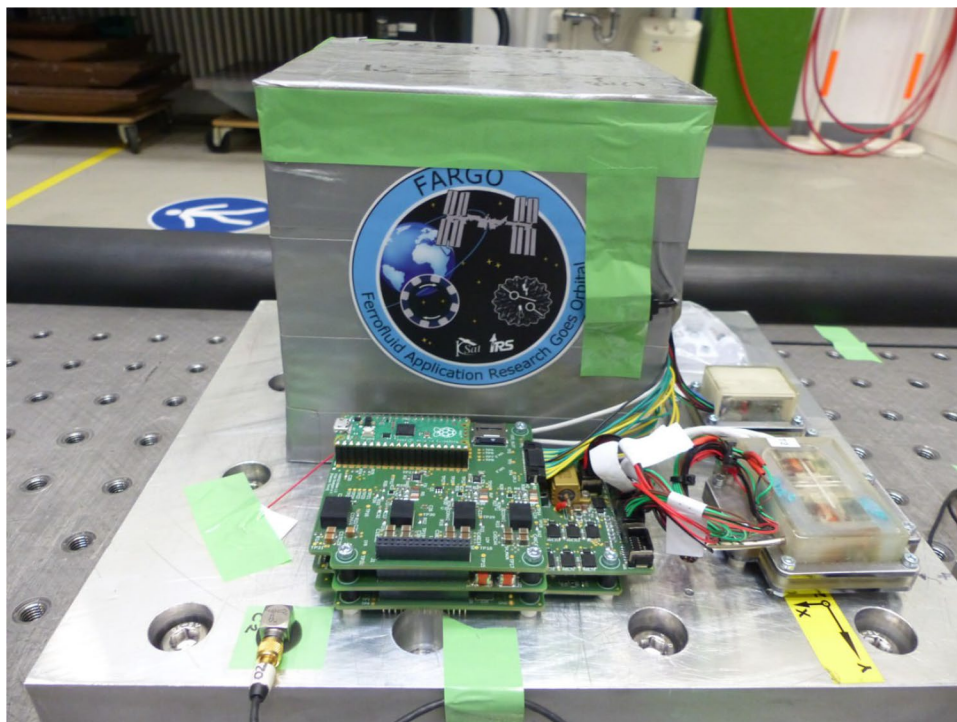
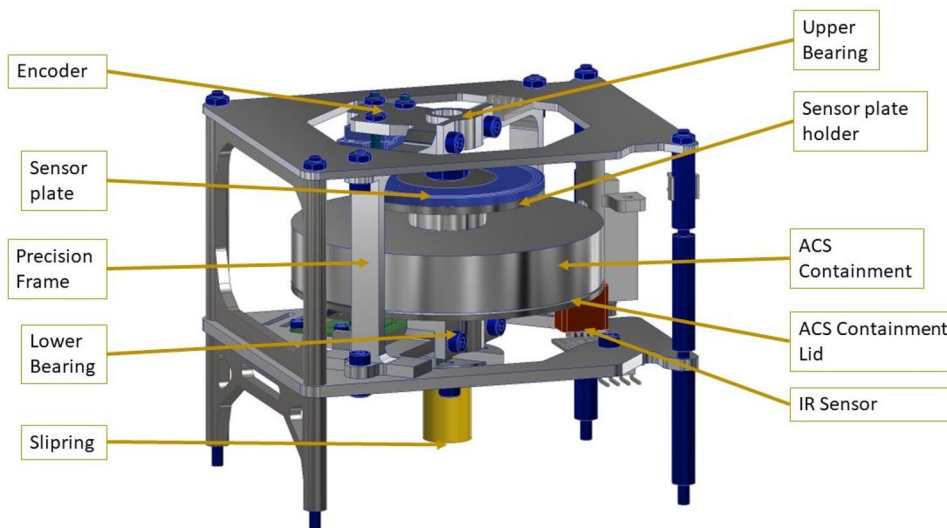


Fig. 18 Angled view of the Ferrowheel experiment CAS with the description of the components.



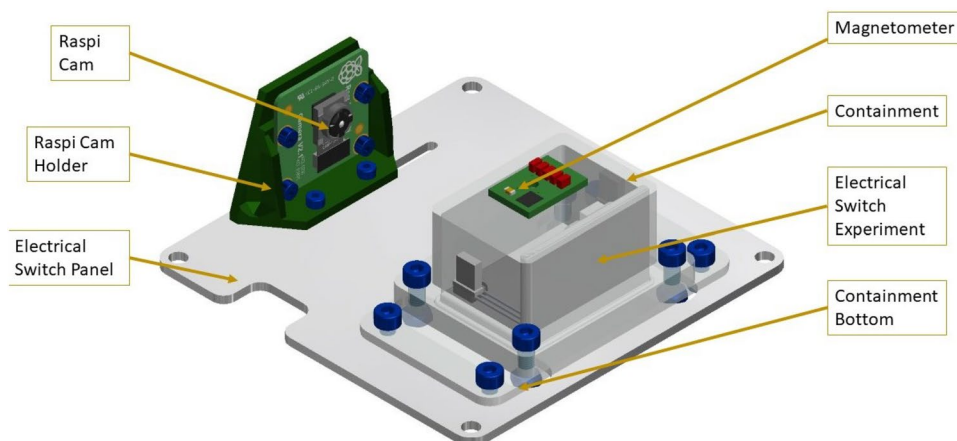
The encoder, used to evaluate the generated torque and the angular momentum storage of the Ferrowheel, is mounted on a sensor mounting plate on top of the experiment; its counterpart, the encoder disc, is fixed onto a custom part directly on top of the Ferrowheel experiment. The slip-ring that is supplying the 3-phase current to the experiment is mounted below the experiment module. A camera is mounted on the lower structural plate, which films into the interior of the ferrowheel. Opposite the camera is an

infrared (IR) sensor that serves as a substitute for the low-resolution encoder in case it fails.

3.1.2 Electrical switch

Both switches are mounted on individual plates. This facilitated the integration process, as it was possible to mount each experiment and all supporting infrastructure on the plate with easy access before integrating it into the main structure. The main part of the experiment consists

Fig. 19 CAD of the Electrical Switch experiment



of a capillary tube filled with ferrofluid and insulating oil, two EPMS and contact materials embedded in the capillary tube to allow current flow. The components are all embedded in an SLA-printed frame that is slid into the polyjet containment for easy manufacturing. The polyjet containment is equipped with an embedded epoxy window on the side facing the camera for enhanced visibility. A detailed overview of the experiment panel CAD is given in Fig. 19.

3.1.3 Thermal switch

Like the Electrical Switch, the Thermal Switch is first mounted onto a panel. The components of the Thermal Switch experiment, namely the capillary containing the ferrofluid, EPMS, sensors and TECs, as well as a heat pipe, are fixed to the polyjet housing and embedded in epoxy. The TECs have to be able to dump their excess heat to be effective as cold/hot ends, so they are connected via a heat pipe that exits the containment. Outside of the containment, it ends in a copper block that

serves as an interface for a copper wick that dumps the heat into the bottom panel. The panel assembly can be seen in Fig. 20.

3.1.4 Electrical compartment

In the electronics compartment (on the bottom panel), three control PCBs and support infrastructure are mounted. As can be seen in Fig. 21, the PCBs are stacked onto the bottom panel. Cables are guided with FDM printed channels. A copper heatsink can be seen in the middle of the panel right next to a fan that is responsible for air circulation in the module alleviating hotspot problems on the PCBs. An important point that was taken as a lesson learned from the previous PABELL project is the early planning of cable ducts and the alignment of the connectors. This experience proved to be very valuable during the design and integration of the electrical components and the cable bundles. All PCBs are coated with a silicone coating from DOWSIL by DOW for environmental- and electrical arc protection.

Fig. 20 CAD of the thermal switch experiment

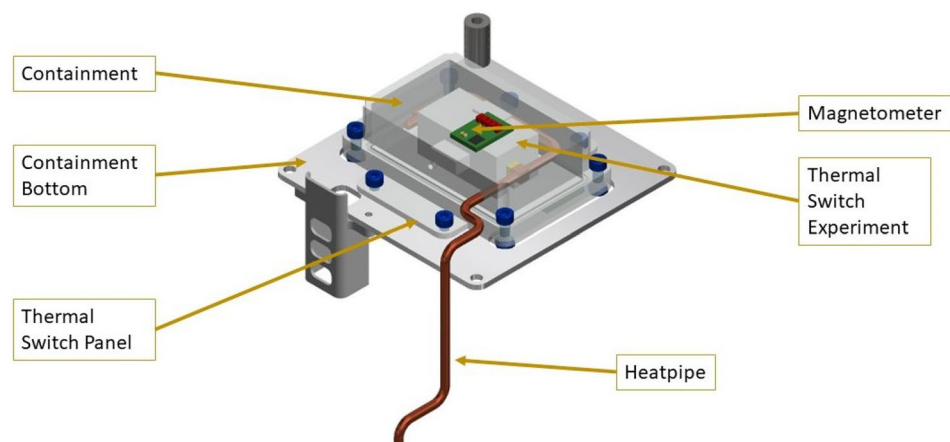
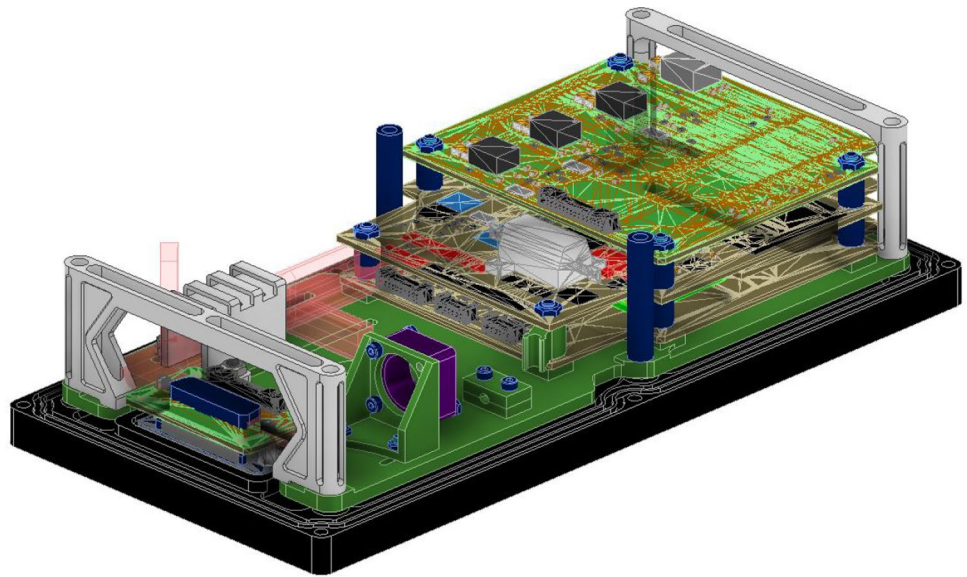


Fig. 21 CAD model of the bottom panel assembly



3.2 Electronics

FARGO is electrically connected to the TangoLab facility, supplying the experiments with the required power

and enabling a downlink of the experiment's data. Various states of both the experiments and the state of the cube can be monitored and reported via housekeeping sensors. The three experiments are controlled by dedicated single-board

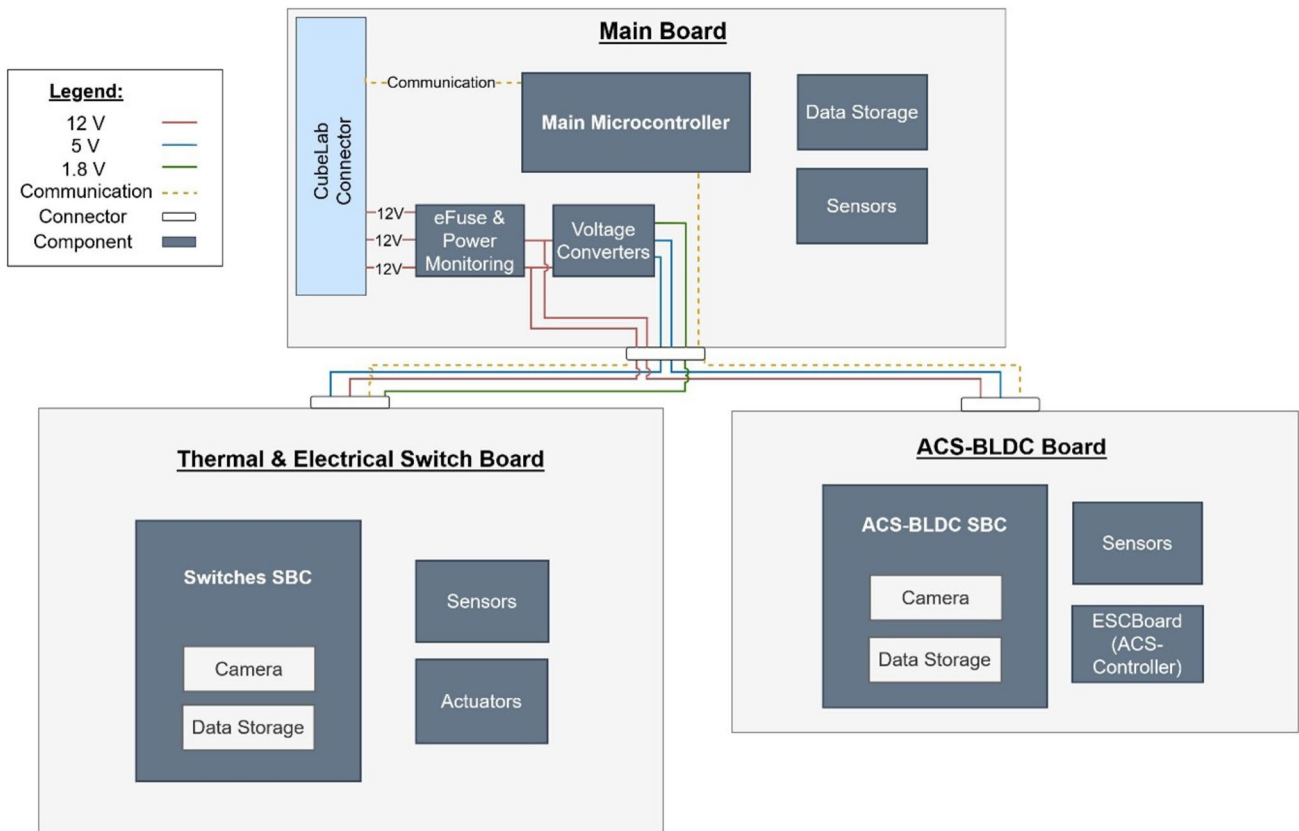


Fig. 22 Overview of the electronics structure chart

computers, which respectively read out the associated sensors and control actuators.

In general, the electronic design is modular, i.e. it consists of the three parts of the main board, the Thermal and Electrical Switchboard and the Ferrowheel board, each either with its own single board computer or a microcontroller, data memories and specific sensors. An overview is shown in Fig. 22. This separation allowed the hardware to be designed and manufactured separately in each of several iterations, and tested individually in the test procedures. The main board serves both as the interface to the SpaceTango facility and as the controller of the experiment sequences. It constantly monitors power consumption. The microcontroller on the main board serves as the main controller, i.e. it is responsible for communicating with the SpaceTango facility. Furthermore, it controls the individual experiment boards via commands, while constantly monitoring them. Finally, the data is collected in the data memory of the main board during the course of the experiments and is thus available to the downlink.

The PCB for the Switches consists of a single-board computer with data storage, a camera and additional electronics to control and monitor the EPMs. In addition, the Thermal Switch uses TECs and an additional coil, which can also be controlled via the switchboard. The critical aspect of driving the EPMs is the short-term high power. They require a voltage peak that is provided by a combination of capacitors and H-bridges. To test the behaviour of the switch under different load characteristics, a resistive load for constant current, a capacitive load for short current spikes, and an inductive load to produce a high voltage

spike are used. The switching characteristics of the Thermal Switch, on the other hand, are evaluated by taking frequent temperature measurements at many different locations on the switch using platinum resistance temperature detectors (RTD) and OneWire temperature sensors. The Ferrowheel board also contains a single-board computer equipped with data storage, a camera, additional sensors and an electronic speed controller (ESC) to control the target speed. To determine the torque generated by the Ferrowheel, the angle of rotation is measured using a high-speed optical incremental encoder by Renishaw. As mentioned earlier, an infrared sensor is also used as a low-resolution backup for angular measurements.

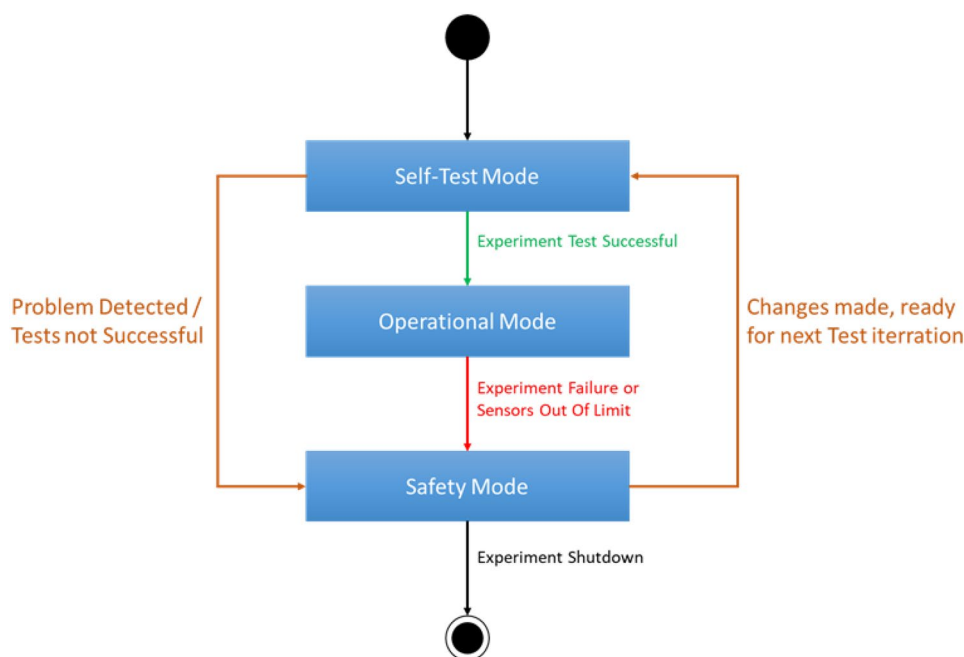
3.3 Software

The software architecture consists of one on-board segment which consists of the main board, the Ferrowheel board and the experiment board for the two switches. All experiment boards are connected to the main board with an SPI bus. Furthermore, the sensor data are collected on the micro-SD card via the SPI bus. The sensors communicate via I2C and OneWire technology.

3.3.1 Modes

For the software of FARGO, different modes are defined that should allow automatic running. The flowchart of the modes is shown in Fig. 23. For each experiment, an

Fig. 23 Defined modes of the software from FARGO



individual operational mode with all sensors and actuators running is defined. In the self-test mode, a verification of basic experiment functions can be obtained, allowing a simple comparison of acquired data from ground experiments. The safety mode, on the other hand, is activated when failure during operation occurs or the experiment time is over, so the experiment shuts down, and a restart is possible.

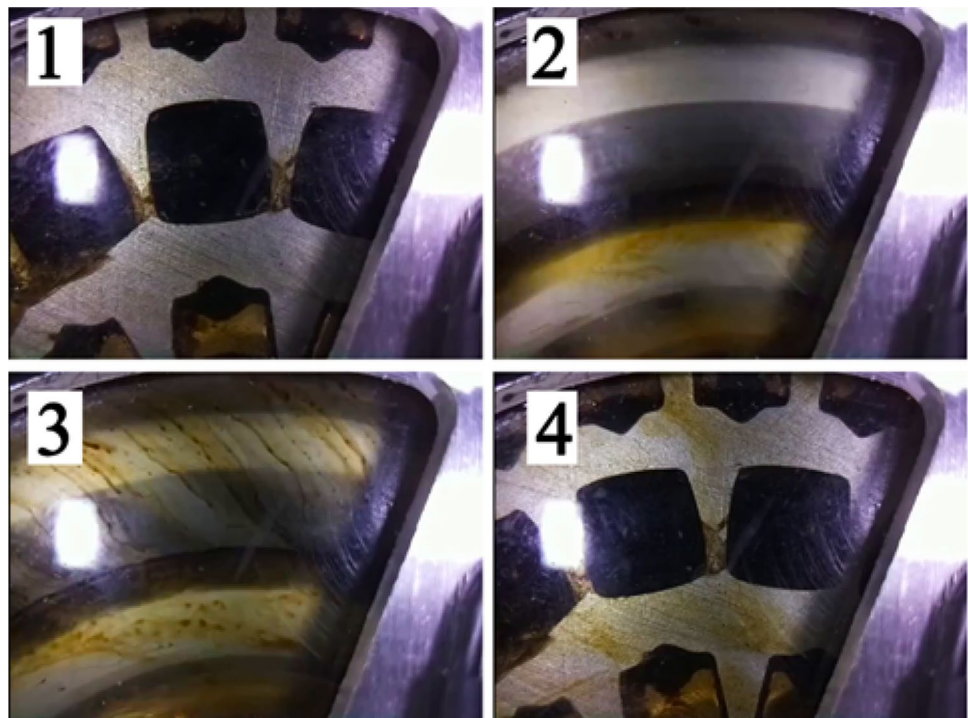
3.3.2 Security concept

To ensure that the probability of transmission or memory problems is as low as possible, Reed–Solomon error correction (RSEC) is used. Since no redundancy can be used for the microcontroller, watchdogs are used for this purpose, which sends a signal to restart the respective experiment board in case of a malfunction of the experiment. In case of repeated malfunction, the individual system will shut down safely. For safety analysis, a combination of System Theoretical Process Analysis (STPA) and Behaviour Driven Development (BDD) is used. BDD is used to test the software for correct implementation, while STPA is used to detect accidents and hazards as unsafe actions and causal factors are identified [40].

4 Operation on the ISS

Following the development time of approximately 1.5 years and after passing all relevant reviews, FARGO was launched aboard the CRS-27 resupply mission using a Falcon 9 rocket on March 15, 2023. Initial operations planning was centered around an autonomous operation of all the experiments and a pre-programmed experiment program, but software problems, especially with the communication between the boards forced a more manual approach. Despite the safety analysis performed beforehand, a reliable autonomous operation was not possible. Although no direct communication with the experiment was possible, SpaceTango provided the possibility to connect to the experiment on a regular basis via SSH and upload files, execute orders and files via the command line. Time shifts and the regular duties of the Space Tango employees enlarged the problems and further limited the communications possibilities. Telemetry was limited due to the experiment’s design focusing on power draw curves. Nevertheless, the operations team managed to deduce the operation status and the state of the sub-experiments, enabling them to respond to off-nominal behaviour and develop mitigation procedures to enhance experiment operation over the course of the 30-day mission. After each experiment run, the data were evaluated and the next script was written based on the initial experiment plan. First, they were tested on a ground model before being then uploaded and tested on the

Fig. 24 Images of the Ferrowheel during operation on the ISS. The motion of the Ferrowheel rotor with the ferrofluid bearing is visible. Panels 1–3 show the increase in the rotation speed, while panel 4 shows the state at a standstill after the operation of the experiment



ISS. This allowed about 30% of the original mission time to be successfully used for experiments.

4.1 Ferrowheel results

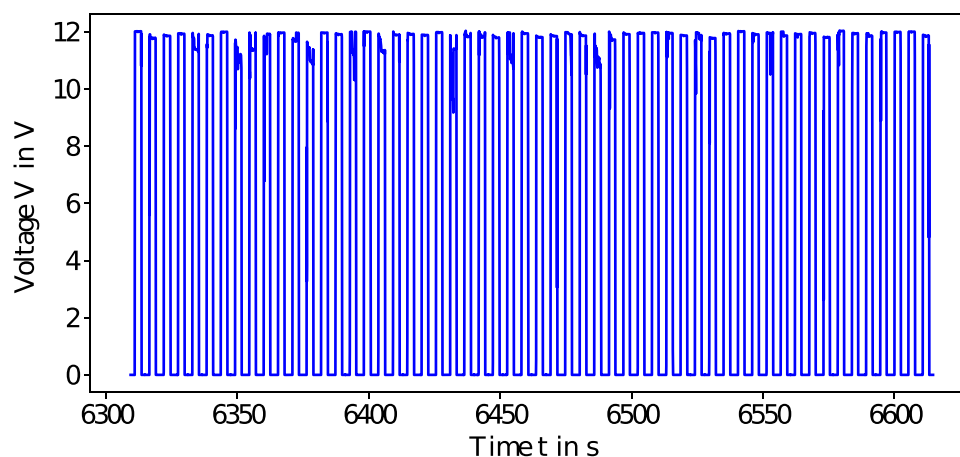
The results described below come from the Ferrowheels encoder and its camera that records the motion. In Fig. 24, four different sequences of images captured provide a step-by-step visualization of the Ferrowheel's operation:

- Shot 1: Displays the ferrofluid cushions, which are strategically positioned on the magnets. These cushions function as bearings within the containment.
- Shot 2: As the disc begins its movement, there's a noticeable spread of the ferrofluid across the containment window.
- Shot 3: At increased RPMs, the ferrofluid undergoes a shift or relocation, which is evident in this image. The emergence of distinct lines underscores this shift.
- Shot 4: This captures the disc at rest once again. The smearing of the ferrofluid, still visible, will eventually diminish. This is attributed to the ferrofluid's inherent tendency to reattach itself to the magnets, showcasing its self-healing property, a unique characteristic of ferrofluidic bearings.

Table 4 Test results of the Ferrowheel conducted on the ISS

	800 RPM	1000 RPM	1100 RPM
Current draw at start (mA)	1280	1380	1380
Initial idling current (mA)	780	810	980
Current [duration] (mA)	720 [11 min]	770 [27 min]	960 [30 min]
No-load current (mA)	360	360	360
Average power draw during operation (W)	4.68	5.16	7.32

Fig. 25 Voltage measurements from the Electric Switch experiment during a load-free switching period of 500 cycles



In idle mode, the Ferrowheel control hardware consumes a current of 360 mA. However, as the system starts up, this consumption increases, peaking at 1280 mA. While operating at a steady RPM of 800, the Ferrowheel's current consumption is initially 780 mA, but this decreases to 720 mA over an 11-min span, as the heating of the ferrofluid by the coils presumably leads to a reduction in viscosity and thus friction. Some test results conducted on the ISS are listed in Table 4.

Comparing these results to ground tests with a similar Ferrowheel setup provides further insights. In these ground tests, the Ferrowheel managed to achieve an RPM of up to 5730 by supplying 12 V. The resulting current draw was approximately 500 mA during startup and 102 mA during idling. Interestingly, the datasheet of the COTS motor states an idle speed of 5730 RPM at 12 V but with a current draw of 127 mA, resulting in 20% less power.

4.2 Electrical Switch results

During the investigations of the Electrical Switch on the ISS, different switching cycles were employed. Besides the current flow, the supplied voltage was also captured. Since reliable switching was not possible at the beginning of the experimental period, the electrical load was switched off to prevent a current flow and to investigate the supplied voltage.

In Fig. 25, the measured voltage for a subset of the 500 switching cycles is measured for this no-load case.

This experiment shows, that the voltage fluctuated from 0 V to approximately 12 V. However, as evident in Fig. 25, some cycles recorded voltage peaks slightly below the supplied voltage. This inconsistency might arise when the Galinstan-ferrofluid drop doesn't fully engage with the electrical contacts inside the capillary during certain switching instances.

In contrast, ensuring uniform motion of the Galinstan-ferrofluid droplet became particularly difficult when the load circuit was closed. In this case, a change in the switching

state of the Electrical Switch did not occur reliably. This could only be circumvented by sending short current pulses through the coil of the EPM when it was switched, resulting in a nearly 100% reliability in the switching state changes. These pulses do not permanently amplify the magnetic field strength of the EPM but are sufficient to ensure full contact with the droplet during switching.

The efficiency of this multi-pulse approach can be seen in Fig. 26, where the pulse count reduces from an initial 128 to just 9 for the concluding cycles.

Figure 27 details the current dynamics during this procedure. It can be concluded, that the initial perception may indicate unsatisfactory switching operations. However, a deeper interpretation validates the efficacy of the implemented

methodology. Observable trends encompass an elevated current surge, immediately followed by a transient current-null period, a subsequent attenuated surge, and another absence of current prior to the inception of the subsequent cycle.

A total of about 700 successful open-loop and 70 closed-loop switching cycles were performed. A comprehensive assessment is essential to discern the fundamental mechanism responsible for the challenges in the attachment and detachment of the drops, whether they are influenced by microgravity conditions or an outcome of the chronological degradation of the Galinstan-ferrofluid drop. The exploration for an appropriate secondary, non-conductive fluid integral for the switch remains in progress, emphasizing its significance for achieving prolonged stability.

Fig. 26 Voltage measurements from the FARGO Electrical Switch experiment with a closed circuit and multiple EPM pulses

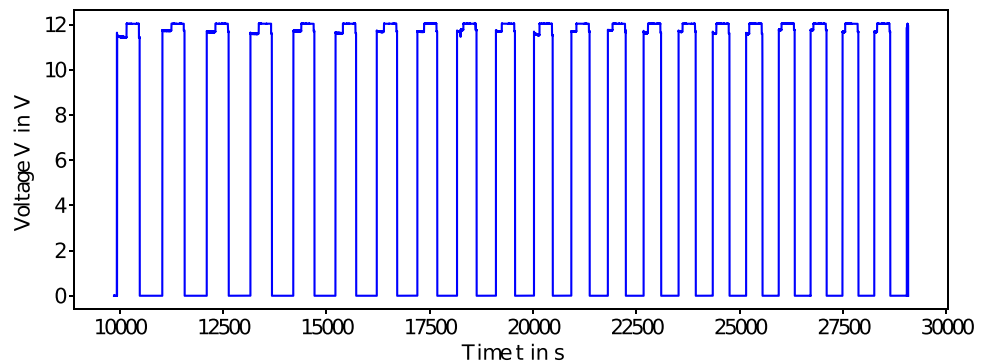


Fig. 27 Current measurement from the FARGO Electrical Switch experiment during switching in a closed circuit with multiple EPM pulses

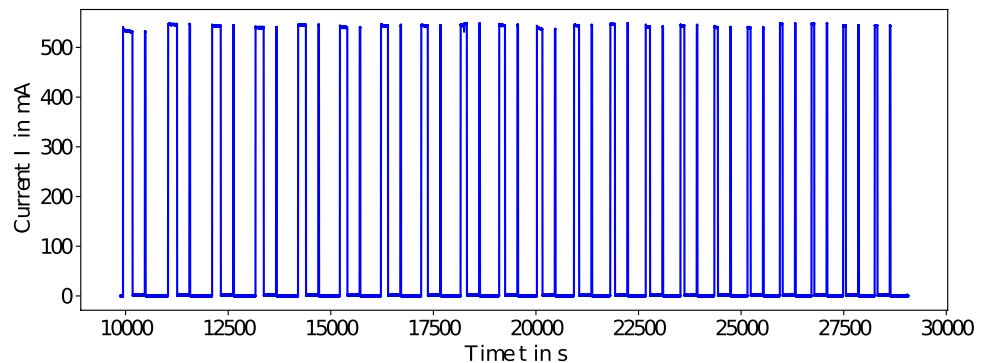
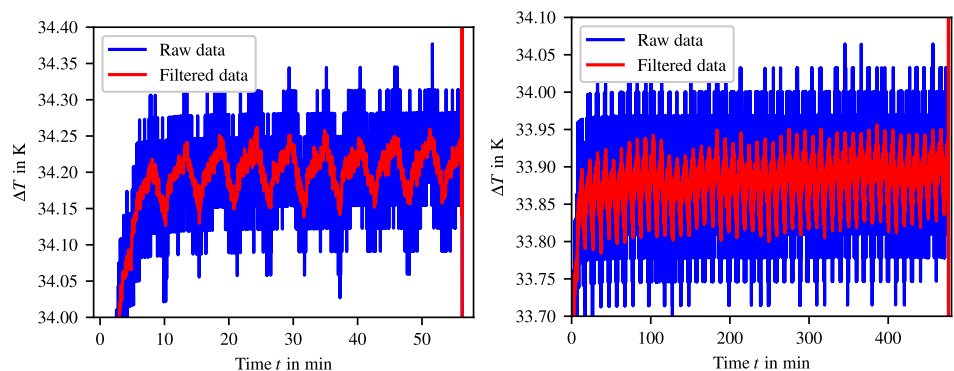


Fig. 28 In the left, the temperature difference ΔT plotted over time for a switching time of 160 s measured during an experimental run on the ISS is plotted. In the right, the switching time is increased to 300 s during a long term experiment with a duration of 8 h. On both data sets, a Savitzky–Golay filter is applied



4.3 Thermal switch results

On the ISS, different switching time cycles were performed with the Thermal Switch experiment. In the left plot in Fig. 28, the temperature disparities, represented as ΔT , are displayed for a switch time of 160 s. The switching impact is evident: temperature difference rises in the OFF state and drops in the ON state. Unfortunately, a stable thermal equilibrium was not reached.

In the right plot in Fig. 28, the Thermal Switch operation had been extended to a longer duration, using a switch time of 160 s over an 8 h experiment. The switching ratio remained consistent throughout and can be determined to $\eta > 1.003$. The difference compared to the switching ratio on the ground with $\eta_{\text{ground}} > 1.04$ can have multiple reasons. First, in microgravity, fluid heat transport solely hinges on conduction. Furthermore, without gravitational influence, surface tension could reshape the fluid droplets. Whereas on Earth, gravity pulls ferrofluid against heat conductors, in space, it might maintain a spherical form, limiting the contact area and thus reducing heat flow. Another reason could be found in the degradation of the fluid, resulting in magnetic nanoparticle agglomeration, decreasing magnetization and the fluid's force. If the ferrofluid doesn't fully align, it minimizes the effective area. Post-mission assessments are still ongoing and further experiments will provide more clarity.

5 Conclusion

The FARGO experiment container was safely returned to Earth and recovered on April 15 aboard the CRS-27 CARGO Dragon spacecraft. On May 17, FARGO arrived back in Stuttgart, where the experiment data could be extracted and processed, and is still ongoing.

In summary, proof-of-concept for microgravity application has been achieved for all three ferrofluid applications. Particularly noteworthy are the electrical and mechanical systems, which functioned fully in the short development and construction phase of about one year and did not exhibit any problems. Only the software was problematic, as listed in Sect. 4, but could be worked around by in-orbit fixes. Considering the short development time and the educational nature of the project, this can nevertheless be considered as project success.

Thus, even though not all tests of the experiments could be performed, the data indicate the successful operation of all three experiments, raising their Technology Readiness Level (TRL) to 6. Currently, the Ferrowheel is being further developed based on the in-orbit results. Evaluations of the current design have already shown an increase in efficiency compared to the specifications of the BLDC

motor. With a re-design, the efficiency of this system is to be increased even further. The Thermal Switch offers the greatest potential for improvement since the use of oil-based ferrofluid instead of liquid metal clearly limits the switching efficiency. Here, ways must be found to develop a design that prevents oxidation of the metal. Furthermore, research is being carried out on a design that makes it possible to fill the area between the contacts better to improve the heat transfer in the on-state of the switch. The Electrical Switch successfully performed a total of about 700 switching cycles with open and 70 cycles with closed loop. However, the switching operation itself was not reliable at the beginning for the reasons mentioned in Sect. 4.2. Research work is pending to improve this.

In addition to further elaboration of the results by team members of KSat e.V., further developments in the field of ferrofluid technologies are pending. For example, in Cycle 14 of DLR's sounding rocket program REXUS, ferrofluid pump technologies are being researched by KSat e.V. in the FERRAS (Ferrofluid Application Study) experiment. Here, the learning experiences gained during FARGO and its predecessor project, PAPELL, are of great importance.

The educational aspects of the FARGO project should also be highlighted. During its development, 23 students from Bachelor's to Master's semesters and from five different degree programs were able to learn hands-on how to develop a real space experiment for the ISS. The opportunities to both apply theoretical knowledge from the curriculum and learn new practical skills are unmatched.

Acknowledgements The FARGO project is made possible by the German Space Agency at the German Aerospace Center (DLR), funded by the Federal Ministry for Economic Affairs and Energy. The Institute of Space Systems of the University of Stuttgart support the project with technical and scientific knowledge and FARGO can use their rooms and technical facilities. The attitude control system is being developed in close collaboration with the FerrAC (Ferrofluid Attitude Control) project funded by the Federal Ministry of Education and Research (grant number: 50RK1973). Furthermore, several companies have sponsored or supported the project like Renishaw, Ginstr, Airbus Defence and Space, Vacuumschmelze, Starke Mineralölwerk, Silikon Profis, IC-Haus, Costenoble and Moflon, Keyence, Ancon, Metallpulver24. A special appreciation should be mentioned for Renishaw, to sponsor us two complete encoder systems. Special thanks is given to Space Tango and their employees for continued support before and during the operations phase.

Author contributions Team FARGO consists of 23 interdisciplinary students, all members of the small satellite student society at the University of Stuttgart, KSat e.V, supported from two PhD students from the Institute of Space System (IRS) at the University of Stuttgart. Furthermore, the project is encouraged by the academic tutors Priv-Doz. Dr. Georg Herdrich and Prof. Dr. Stefanos Fasoulas from the IRS. The team has formed from members of the small satellite student society at the University of Stuttgart, KSat e.V. In total, five fields of studies are represented—from aerospace engineering, physics, chemistry, electrical engineering and software.

Funding Open Access funding enabled and organized by Projekt DEAL. The project is made possible by the Überflieger2 competition funded by the German Space Agency at DLR.

Availability of data and materials All data and materials can be used in agreement with the authors or by declaration.

Code availability Not applicable.

Declarations

Conflict of interest The authors declare that there are no conflicts of interest.

Open Access This article is licensed under a Creative Commons Attribution 4.0 International License, which permits use, sharing, adaptation, distribution and reproduction in any medium or format, as long as you give appropriate credit to the original author(s) and the source, provide a link to the Creative Commons licence, and indicate if changes were made. The images or other third party material in this article are included in the article's Creative Commons licence, unless indicated otherwise in a credit line to the material. If material is not included in the article's Creative Commons licence and your intended use is not permitted by statutory regulation or exceeds the permitted use, you will need to obtain permission directly from the copyright holder. To view a copy of this licence, visit <http://creativecommons.org/licenses/by/4.0/>.

References

1. AEGIS: In space, no one can hear your bearings fail. <https://blog.est-aegis.com/in-space-no-one-can-hear-your-bearings-fail>. Accessed 11 Sept 2022
2. NASA: Galileo FAQ - Galileo's Antenna. <https://www2.jpl.nasa.gov/galileo/fahga.html#why>. Accessed 11 June 2023
3. Space product assurance. ECSS Q-HB-30-08A, European Space Agency (2011)
4. Handbook of reliability prediction procedures for mechanical equipment. Handbook, Naval Surface Warfare Center (2011)
5. Papell, S.S.: Low viscosity magnetic fluid obtained by the colloidal suspension of magnetic particles. US3215572A (1963)
6. NASA: Novel rocket fuel spawned ferrofluid industry. <https://www.nasa.gov/feature/glenn/2021/history/novel-rocket-fuel-spawned-ferrofluid-industry>. Accessed 12 Sept 2022
7. Datta, P.: Magnetic gels, pp. 441–465 (2018). <https://doi.org/10.1016/B978-0-08-102179-8.00017-X>
8. Lange, A., Langer, H., Engel, A.: Dynamics of a single peak of the Rosensweig instability in a magnetic fluid. *Physica D* **140**(3), 294–305 (2000). [https://doi.org/10.1016/S0167-2789\(00\)00018-X](https://doi.org/10.1016/S0167-2789(00)00018-X)
9. Breitenbuecher, L.: Assessment of ferrofluid interaction with secondary liquids. Bachelor thesis, Institute of Space Systems, University of Stuttgart (2019)
10. Breitenbücher, L., Sütterlin, S., Ehresmann, M., Schäfer, F., Herdrich, G., Fasoulas, S.: Assessment of ferrofluid interaction with secondary liquids. In: 71st international astronomical congress, IAC (2020)
11. Ferrotec: Safety data sheet. <https://ferrofluid.ferrotec.com/wp-content/uploads/sites/3/efhsds.pdf>. Accessed 12 Sept 2022
12. Suetterlin, S.: Design and analysis of electrical and thermal ferrofluid switches. B.s. thesis, Institute of Space Systems, University of Stuttgart (2020)
13. Hu, L., Wang, H., Wang, X., Liu, X., Guo, J., Liu, J.: Magnetic liquid metals manipulated in the three-dimensional free space. *ACS Appl. Mater. Interfaces* **11**(8), 8685–8692 (2019). <https://doi.org/10.1021/acsami.8b22699>
14. PSE Online: Das Periodensystem der Elemente online. <http://www.periodensystem-online.de/index.php?el=31>. Accessed 01 Sept 2022
15. Anwar, M.S., Ehlers, F., Bangert, A.: Experimental analysis of liquid metal Galinstan for electronics actuation. *Electron. Lett.* **58**(16), 617–619 (2022). <https://doi.org/10.1049/el12.12541>
16. Fisk, M.: In: Hetnarski, R.B. (ed.) *Induction Heating*. Springer, Dordrecht (2014)
17. Dietrich, J.: Development of a ferrofluidic electric switch for in space operation. B.Sc. thesis (2022)
18. VAC: Nickel-Eisen Legierungen. <https://vacuumsmelze.de/Produkte/Weichmagnetische-Werkstoffe-und-Stanzteile/40-bis-50-Nickel-Eisen>. Accessed 01 Dec 2020
19. Knaian, A.N.: Electropermanent magnetic connectors and actuators: devices and their application in programmable matter. Ph.D., MIT, Massachusetts Institute of Technology, Massachusetts (2010)
20. University of Hannover: "Gluecksklee" auf der Internationalen Raumstation. <https://www.et-inf.uni-hannover.de/de/aktuelles/news/aktuelles-detailansicht/news/gluecksklee-auf-der-internationalen-raumstation/>. Accessed 14 Sept 2022
21. WARR e.V.: Addoniss Mission - WARR. <https://warr.de/en/projects/spacelabs/addoniss/>. Accessed 14 Sept 2022
22. University of Luxembourg: BRAINS—Uni students will conduct experiment in space. https://www.uni.lu/snt/news_events/brains_uni_students_will_conduct_experiment_in_space. Accessed 14 Sept 2022
23. SpaceTango: CubeLab. <https://spacetango.com/cubelab/>. Accessed 14 Sept 2022
24. Weppler, J., Lemack, C., Steinpilz, T., Musiolik, G., Kruss, M., Demirci, T., Jungmann, F., Kraemer, A., Tappe, J., Aderholz, M., Teiser, J., Wurm, G., Koch, T., Schaper, Y., Nowok, R., Beck, A., Christ, O., Genzel, P., Lindner, M., Matschey, Y., Leber, D., Rempt, S., Schmuck, F., Spahr, D., Winkler, B., Brenker, F., Hild, F., Grunwald, K., Ehresmann, M., Suetterlin, S., Heinz, N., Aslan, S., Grabi, F., Sauer, M., Schweiger, R., Herdrich, G.: Ueberflieger—a student competition for ISS experiments. In: 68th international astronomical congress (2017)
25. Ehresmann, M., Hild, F., Suetterlin, S., Heinz, N., Boelke, D., Hofmann, S., Grundwald, K., Behrmann, C., Herdrich, G., Jemmal, R.: Experiment results and post-flight analysis of the ISS student experiment PAPELL. In: 70th international astronomical congress, IAC (2019)
26. Heinz, N.: Concept study of a piston pump based on ferrofluid manipulation. Bachelor thesis, Institute of Space Systems, University of Stuttgart (2020)
27. Schneider, M.: Development of additively manufactured stators for ferrofluid manipulation. Bachelor thesis, Institute of Space Systems, University of Stuttgart (2020)
28. Schäfer, F., Ehresmann, M., Herdrich, G., Fasoulas, S.: Update on the development of FerrAC the mechanic-free attitude control system. In: 71st international astronomical congress, IAC (2020)
29. Korn, C.: Design and manufacture of a torque measuring test-bed for experimental attitude control actuators. Bachelor thesis (2020)
30. Ehresmann, M., Sütterlin, S., Bölke, D., Heinz, N., O'Donohue, M., Remane, Y., Kreul, P., Schneider, M., Korn, C., Dietrich, J., Wank, B., Zajonz, S., Kob, M., Großmann, S., Philipp, D., Turco, F., Buchfink, M., Steinert, M., Acker, D., Fasoulas, S.: An innovative wearless attitude control actuator based on ferrofluid manipulation tested on the ISS. In: 34th International Symposium on Space Technology and Science, ISTS (2023)

31. Ferrotec: APG 300 Series Ferrofluid, Type: APG 313. <https://ferrofluid.ferrotec.com/products/ferrofluid-audio/apg-300-series/apg-313/>. Accessed 02 Sept 2023
32. Ferrotec: APG CDF Series Ferrofluid, Type: APG CDF 2250. <https://ferrofluid.ferrotec.com/products/ferrofluid-audio/apg-cdf/apg-cdf-2250/>. Accessed 02 Sept 2023
33. Ferrotec: EFH Series Educational Ferrofluid, Type: EFH1. <https://ferrofluid.ferrotec.com/products/ferrofluid-educational-fluid/efh/efh1/>. Accessed 08 Sept 2023
34. Lee, K., Kim, D.: Thermomagnetic convection of ferrofluid in an enclosure channel with an internal magnetic field. *Micromachines* **10**, 553 (2019). <https://doi.org/10.3390/mi10090553>
35. Kuchler, A.: *Hochspannungstechnik*. Springer, Heidelberg (2009). <https://doi.org/10.1007/978-3-540-78413-5>
36. Starke Mineralölwerk: StaSo Transformatorenöl I. Technical report
37. RS: JWD JWS Series. <https://docs.rs-online.com/3075/0900766b8122cddb.pdf>. Accessed 04 Dec 2020
38. NL1020T single-stage thermoelectric module. https://cdn2.hubspot.net/hubfs/547732/Data_Sheets/NL1020T.pdf. Accessed 28 May 2020
39. Kob, M., Karahan, B., Sütterlin, S., Dietrich, J., Bölke, D., Steinert, M., Heinz, N., Gutierrez, E., Großmann, S., Philipp, D., Turco, F., Buchfink, M., Korn, C., Zajonz, S., O'Donohue, M., Remane, Y., Kreul, P., Schneider, M., Acker, D., Herdrich, G.: Fargo in-orbit verification of a thermal switch in ISS microgravity (2023)
40. Steinert, M.: Design and implementation of software tests for the ISS-experiment FARGO based on STPA-BDD. Master's thesis (2022)

Publisher's Note Springer Nature remains neutral with regard to jurisdictional claims in published maps and institutional affiliations.

Authors and Affiliations

Saskia Sütterlin^{1,2} · Daniel Bölke² · Manfred Ehresmann^{2,3} · Nicolas Heinz² · Janoah Dietrich² · Bahar Karahan² · Maximilian Kob² · Michael O'Donohue² · Christian Korn² · Steffen Grossmann² · Daniel Philipp² · Michael Steinert² · Denis Acker² · Yolantha Remane² · Phil Kreul² · Maximilian Schneider² · Sebastian Zajonz² · Bianca Wank² · Fabrizio Turco² · Manuel Buchfink² · Elizabeth Gutierrez² · Sonja Hofmann² · Silas Ruffner² · Alexander Wagner² · Laura Breitenbücher³ · Felix Schäfer^{2,3} · Georg Herdrich³ · Stefanos Fasoulas³

✉ Saskia Sütterlin
suetterlin@ksat-stuttgart.de

³ Institute of Space Systems, University of Stuttgart,
Pfaffenwaldring 29, 70569 Stuttgart, Germany

¹ University of Stuttgart, Stuttgart, Germany

² Team FARGO, Small Satellite Student Society KSat e.V.,
Pfaffenwaldring 29, 70569 Stuttgart, Germany